Computers and Structures 243 (2021) 106399

Contents lists available at ScienceDirect

Computers and Structures

journal homepage: www.elsevier.com/locate/compstruc

Computational modeling of three-dimensional mixed mode-I/II/III fatigue crack growth problems and experiments

Ali O. Ayhan [a,*], Oğuzhan Demir [a,b]

[a] Department of Mechanical Engineering, Sakarya University, 54050 Sakarya, Turkey
[b] Department of Mechanical Engineering, Bilecik Seyh Edebali University, 11210 Bilecik, Turkey

ARTICLE INFO

Article history:
Received 10 December 2019
Accepted 19 September 2020
Available online 23 October 2020

Keywords:
Computational fatigue crack propagation
Mixed mode-I/II/III
Non-planar crack growth
Three-dimensional crack growth criterion

ABSTRACT

Mixed mode-I/II/III fatigue crack growth experiments and their simulations are performed using a system permitting all possible combinations of three-dimensional mixed mode loading conditions. The so-called Compact Tension-Shearing and Tearing (CTST) specimens used in the experiments are made of 7075-T651 aluminum alloy. Different mixed mode loading conditions are considered and the applicability of a previously developed new 3-D fracture criterion on 3-D mixed mode fatigue problems is evaluated. Crack growth surfaces obtained from numerical simulations and experiments are compared using existing criteria in the literature and the developed criterion. Especially for highly mixed mode conditions, the developed criterion predicts the crack growth surface better than the MTS criterion by reducing nearly half of the latter's deviation from the experimental surface. Based on the computed mixed mode stress intensity factors, comparisons of lives show that most mixed mode fracture criteria underpredict fatigue crack propagation lives. Numerical analyses are also performed on a cylindrical steel bar under combined tension–torsion fatigue load to further validate the method presented. The predicted results showed good agreement with experimental data from the literature.

© 2020 Elsevier Ltd. All rights reserved.

1. Introduction

One of the main reasons for crack formation, fatigue crack growth (FCG) and fracture problems encountered in practical engineering applications is the exposure of structural and/or machine parts to high magnitudes of complex fatigue loadings. Most studies in the literature related to fatigue crack growth mainly focused on crack growth behavior under pure mode-I loads acting perpendicular to the crack plane and two-dimensional mixed mode-I/II loads, under which the crack propagates through a curved path in its plane. However, it can also be frequently observed that a crack in an engineering application can also be subjected to combinations of modes –I, -II and -III loads, resulting in mixed mode-I/II/III loading with all three active fracture modes. In such a situation, a crack can propagate under fatigue loading or it can fracture in a three-dimensionally non-planar manner depending on geometry, loading direction and boundary conditions of the problem. From the perspective of being able to predict three-dimensional FCG, modeling, mesh generation and incremental crack propagation analyses of non-planar cracks are much more complex than those of mode-I and two-dimensional mixed mode-I/II propagation problems. In order to predict incrementally successive crack front profiles during a crack propagation simulation, equivalent stress intensity factor (SIF) values, crack growth deflection angle and crack growth amount for each nodal point on the respective 3-D curved crack front need to be determined by separate equations. These equations are developed as a function of three fundamental SIFs, i.e., K_I, K_{II} and K_{III}, and play a key role in the simulation described above.

Under mixed mode loading conditions, mode-II and mode-III fracture modes are coupled with each other. Due to the bending effect of mode-III (tearing) loading in the out-of-plane direction, additional K_{II} SIFs are induced along the crack front and due to the Poisson's ratio effect of the material, mode-II (in-plane shear) loading results in additional K_{III} SIFs along the crack front. Therefore, the underlying mechanisms acting under general three-dimensional mixed mode loading are complex and highly interactive. Although the coupled modes have been known and observed numerically for many years [1–3], they may not be specifically dealt with in some theoretical and experimental considerations [4–9]. The effect of these coupled modes must be elucidated distinctly. Several stress or energy-based 3-D failure criteria are developed so far to determine fracture behavior of the cracked structures under general mixed mode loading conditions. Some of them are Pook [10], Richard et al. [11], and Schollmann et al.

* Corresponding author.
E-mail address: ayhan@sakarya.edu.tr (A.O. Ayhan).

https://doi.org/10.1016/j.compstruc.2020.106399
0045-7949/© 2020 Elsevier Ltd. All rights reserved.

[12] criteria, which were proposed for the prediction of crack kinking and twisting angles and equivalent SIF. Irwin [13], Sih [14], Tanaka [15], and Kikuchi et al. [16] also developed equivalent SIF equations by using the three modes of SIFs. In our recent previous studies [17,18], numerical and experimental mixed mode-I/II/III fracture analyses were performed and critical fracture loads obtained from the tests were compared with 3-D criteria mentioned above. The results showed that all of the existing criteria underestimated the fracture loads for high mode mixity cases, in which the coupled modes are dominant. Therefore, it is necessary to evaluate the 3-D fracture criteria with extensive numerical and experimental studies. Other than the above recent studies [17,18], in order to investigate mixed mode-I/II/III fracture phenomena by using conventional axial test machine only a few types of loading apparatus had been proposed in the literature [2,19–23]. However, monitoring of crack length and its propagation required for FCG experiments is either impossible or limited on these test apparatus due to their design styles.

One of the aspects of 3-D fracture and fatigue crack propagation is the free-surface effect. It is well known that at the point where the crack front intersects the free surface, the stress singularities are a function of the angle of intersection and Poisson's ratio [24–29]. As noted in [27], the corner point singularity only dominates within a limited region, so in some circumstances, a corner point singularity region may lie within a *K*-dominated region and that the size of the corner region (boundary layer) in which the crack tip stress field is characterized by the stress intensity measure is not generally known. Therefore, in this study, no special treatments are made to the free-surface SIF values other than extrapolating from the crack front point in the close vicinity of the free-surface, after which the free-surface effect is seen on the SIF distribution. Based on Ref. [29] it is worthwhile to note that, using FE models mixed mode SIFs near the free-surface are calculated and defined correctly within some small distances from the free-surface, which supports the approach described above.

In order to provide small scale yielding conditions under LEFM (Linear Elastic Fracture Mechanics) rules, before performing mixed mode tests the required specimen thickness ($t \geq 2.5(K_{IC}/\sigma_y)^2$) was computed according to ASTM E399 standard [30] using results from finite element analyses of the mixed mode specimen used in this study under different loading conditions. The required thickness was computed as 8–10 mm for plane strain mode-I fracture conditions. To fracture the specimen for high mode mixity conditions, the required load levels and plastic zone size increase. As a consequence, to provide small scale yielding conditions under LEFM rules, the required specimen thickness also increases. Therefore, specimens with 25 mm thickness (which is 2.5 times more) were used in the mixed mode fracture experiments. Furthermore, it is also noted that in the current study, magnitudes of the applied fatigue loads are much less than the corresponding fracture loads to break the specimens.

One other aspect for 3-D fracture is the out-of-plane constraint, especially for elasto-plastic materials. There are studies in the literature that investigate detailed stress distributions ahead of mode-I and mixed mode crack fronts by taking into account in-plane and out-of-plane constraint effects [31–35]. Ref. [35] demonstrated that for thick specimens (t/w = 0.5, t: thickness, w: width of the specimen), the out-of-plane constraint effect is almost zero. In the present work, thick specimens (t/w = 0.5) made of Al-7075 exhibiting brittle fracture behavior are used and their fatigue crack propagation behaviors are assessed in terms of mixed mode stress intensity factors by compatibly using numerical [17] and experimental [18] results representing the same mixed mode-I/II/III fracture test system with no consideration of crack tip constraint effects.

In the recent previous studies [17,18], only the fracture aspect of 3-D mixed mode crack problems were investigated and related fracture criteria were developed. In this study, mixed mode-I/II/III FCG experiments are performed by using the recently developed loading fixture [17,18], which permits all possible combinations of mixed mode loading, and the optical measurements required for monitoring of crack.

Fatigue crack propagation analyses are carried out by using combined failure criteria, in which the equation of crack deflection angle was developed from mixed mode-I/II tests [36] and the equation of equivalent SIF was developed from mixed mode-I/III and mixed mode-I/II/III tests [18]. FCG surfaces and lives obtained from numerical and experimental analyses are compared for different mode mixity ratios.

In this paper, computational fracture mechanics simulations of fully three-dimensional mixed mode-I/II/III fatigue crack growth experiments are carried out. Applicability of a new 3-D fracture criterion is evaluated using the results of mixed mode-I/II/III experiments under fatigue loading. Excellent agreement is observed between fatigue crack growth surfaces obtained from experiments and those predicted by the simulations using the developed criterion. Although close predictions by the developed criterion are obtained for non-planarly evolving 3-D fatigue crack growth surfaces and for estimation of the final unstable fracture point under all loading angles, the predicted fatigue lives using the developed and different existing criteria in the literature are far away from the experimental data. This contradictory result is comprehensively discussed at the end of Section 4.

The present work is organized as follows: In the next section, details of a recently developed mixed mode-I/II/III test system and description of the fatigue crack growth test procedure are given. Section 3 investigates the results of three dimensional mixed mode fatigue crack growth analyses performed using 3-D enriched finite element analyses and the recently developed 3-D fracture criterion [18]. Comparisons of the experimental fatigue crack growth lives with those predicted by the developed and existing criteria are given in Section 4. An independent validation example demonstrating the usage of the developed criterion is presented in Section 5. Finally, summary and conclusions are drawn in Section 6.

2. Mixed Mode-I/II/III fatigue crack growth experiments

Fatigue crack growth experiments are performed by using Compact Tension-Shearing and Tearing (CTST) specimen (Fig. 1) under different combinations of mixed mode-I/II/III loading conditions. In order to simultaneously generate all of mode-I, mode-II and mode-III external loads on the specimen at desired individual levels, a loading apparatus (Fig. 2), which was used in conjunction with the CTST specimen in the previous research [17,18] for mixed mode-I//II/III fracture analyses and experiments, is used. Detailed dimensions for the parts of the apparatus can be found in [17]. The Al 7075-T651 alloy machined from rolled plates in the L-T rolling direction is used as the CTST specimen material, which has an elastic modulus of 70GPa, a Poisson's ratio of 0.33 and an initial yield stress of 500 MPa. The loading apparatus and bolts are made of St 4140 steel and HSS steel, respectively (Fig. 2). Young's modulus and Poisson's ratio of the loading devices and bolts are 200 GPa and 0.3, respectively. In Fig. 2, overall view of the test assembly with its parts is shown. The arch-shaped (A) part allows the loading axis to pass through the mid-point of the specimen loading holes under different loading angles varying from 0° to 90° in steps of 15°. The single-grip flange (B) part, which provides axial alignment of the system along the loading axis of the test machine and produces out-of-plane loading on the specimen when rotated,

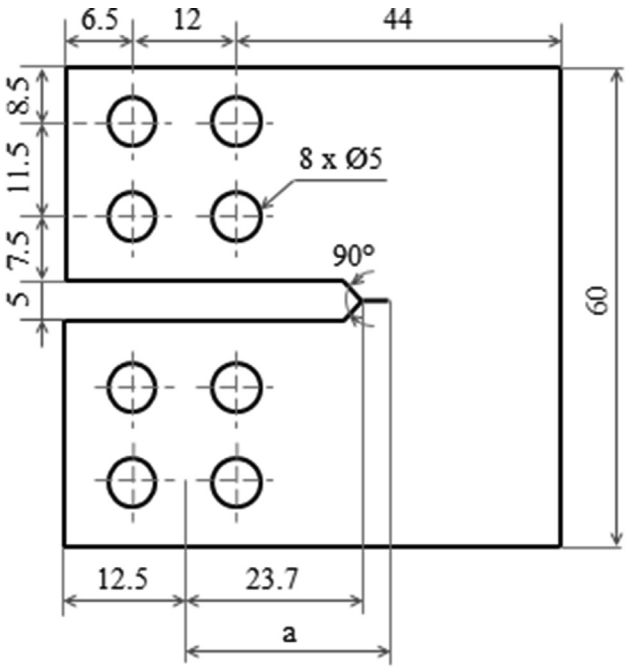

Fig. 1. Dimensions of the CTST specimen (thickness is 25 mm, [17,18]).

is attached to the arch-shaped (A) part and to the specimen via the tightly screwed bolts. To allow introduction of different levels of out-of-plane loading on the tested specimen, bolt holes with steps of 15° are created around the flange (B). By rotating the single-grip flange (B) part attached to the specimen around "*y*" axis and by clamping the mode-I clevis of the test machine on the desired loading hole on the arch-shaped (A) part, any combinations of modes-I, -II and -III can be generated on the specimen. A given 3-D mixed mode general loading generated on the specimen is described as follows: For the case of rotation around "*y*" axis by angle α, and, clamping the mode-I clevis of the test machine on the arch-shaped (A) part by angle β, the loading case is symbolized as, M−II/III = α, M−I/II = β, M−I/III = β (Fig. 2). In order to start the 3-D mixed mode FCG test with a sharpened crack, for all tested specimens, first fatigue precracking is performed under pure mode-I tensile loading according to ASTM E647-13a standard [37]. In the absence of any standard requirement for the loading levels of a pre-cracking process before 3-D mixed mode fracture or fatigue tests, in a compatible manner with the standard for mode-I FCG tests [37], precracking loads are applied such that the final K_{max} during precracking doesn't exceed the initial equivalent K_{max} of the upcoming mixed mode FCG tests. Needless to say that these equivalent SIF values are calculated using the computed mixed mode SIFs from 3-D finite element analyses described in the following section. Compression precracking is another alternative test method for generating fatigue crack growth threshold data, without appreciable load-history effects [38,39]. However, as noted in [39], recent studies showed that the residual stress field arising from compression loading affects crack growth rates during the test following the compression precracking.

After precracking, mixed mode fatigue crack growth tests are performed by positioning the loading apparatus using the desired two independent loading angles. All tests presented in this study are performed at the stress ratio (R) of 0.1. Monitoring and measurements of crack propagation during tests are done by simultaneously recording at predetermined time intervals the front and back-side images of the specimen's crack tip region from high-zoom cameras and the number of cycles associated with the corresponding crack length and growth state. The cameras, which are used to monitor the positions of front and back surface crack tips and to measure the crack lengths, had a magnification capacity of 800X and a manual focus range from 0 mm to 200 mm. In all experiments, 25 mm-thick specimens are used. General views of the experimental set-up for different loading angles are given in Fig. 3. Strain gage measurements had also been performed to determine the accuracy of the finite element simulations involving

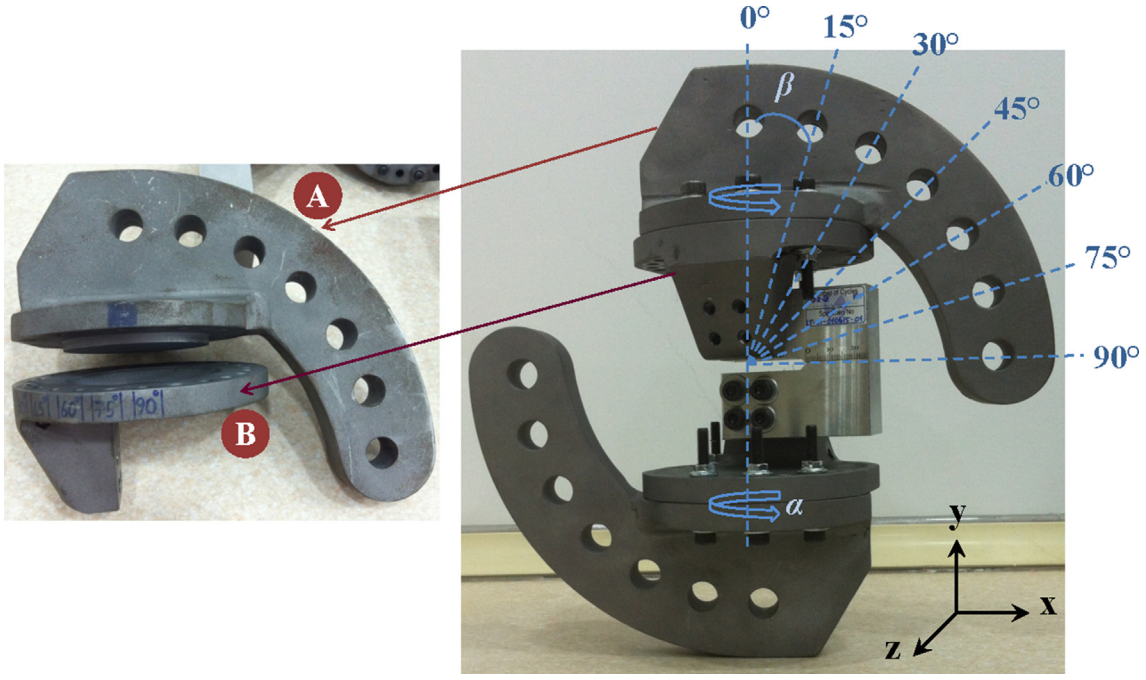

Fig. 2. Mixed mode-I/II/III test assembly and loading angles.

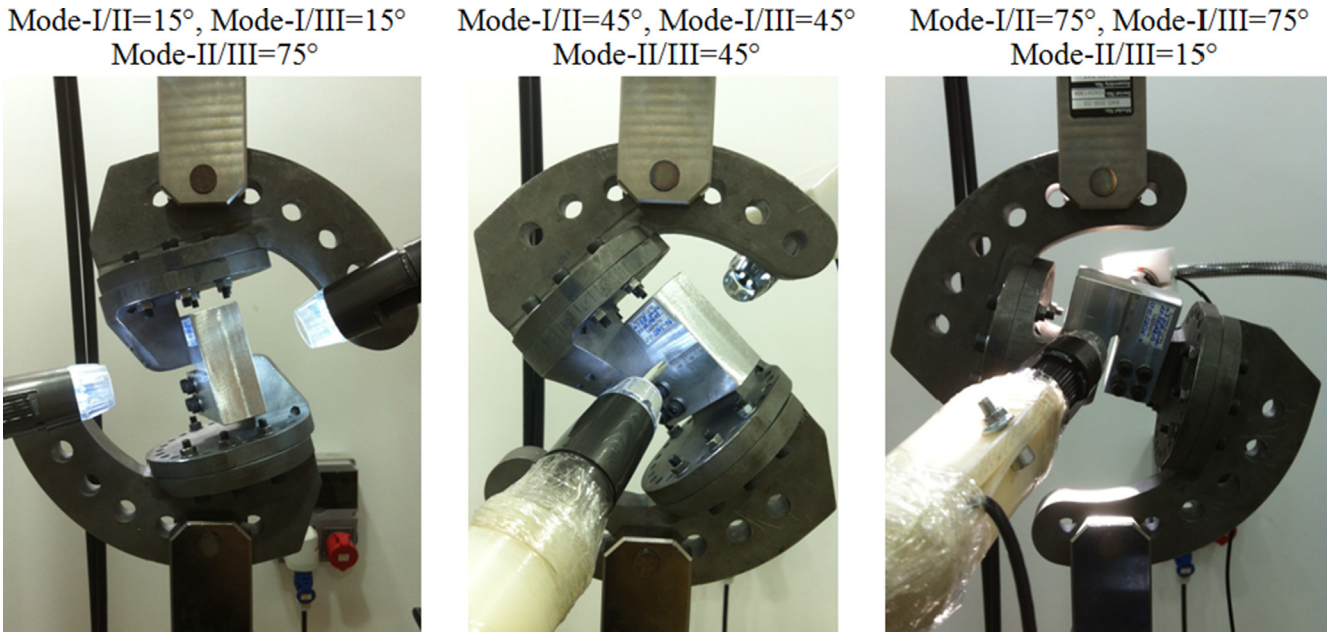

Fig. 3. Views of the experimental set-up for different loading angles.

contact mechanics between contacting surfaces in the test assembly and good agreement had been obtained with the analysis results [18].

3. Three dimensional mixed mode fatigue crack growth analyses

3.1. Analysis method

In this sub-section, the analysis procedure for simulation of mixed mode-I/II/III fatigue crack growth tests is described. The process steps of the analysis procedure are given in Fig. 4. ANSYS™ [40] is used to generate all finite element models employed in the study and to perform their stress analyses, which involve the appropriate contact mechanics as part of the physiscs of the problem. Experimental fatigue crack growth surfaces from the broken specimens are scanned in order to start the crack growth simulation analyses with the actual mode-I pre-crack lengths of the specimens tested under different mixed mode-I/II/III loading conditions and to compare the predicted simulation surfaces with experimental surfaces. In Fig. 5, overall and exploded views of the finite element model of the test assembly with boundary conditions and

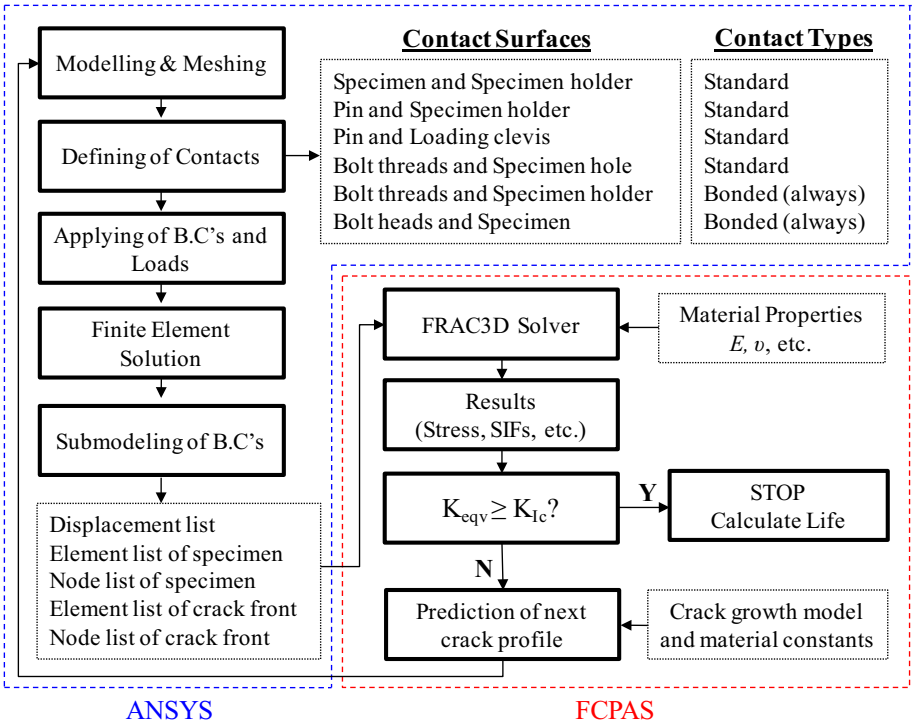

Fig. 4. The process map of fatigue crack growth analysis procedure.

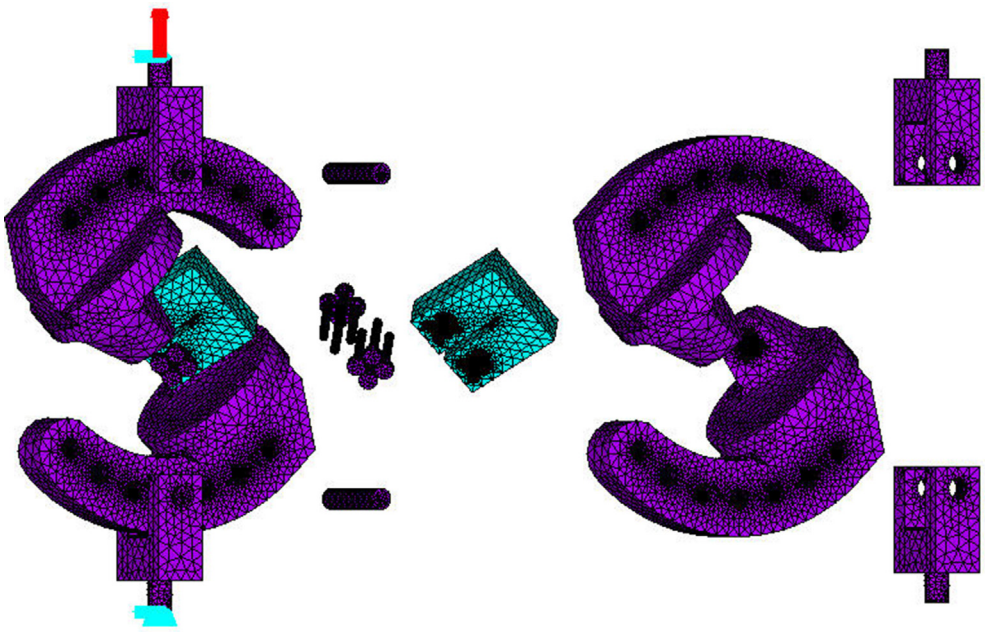

Fig. 5. Overall and exploded views of the finite element model for an arbitrary loading angle.

loads are presented for an arbitrary loading angle. The finite element meshes are generated using 10-noded tetrahedral elements in the whole model, including the regions along the crack front. Typical mesh convergence studies are employed and as a mesh refinement parameter, ratio of crack length (a) and crack tip element size (*Stip*), in perpendicular directions to the crack front is found to be appropriate such that $a/Stip$ = 100. The model shown in Fig. 5 had a total of 307,298 10-noded tetrahedral elements and 433,265 nodes. Boundary conditions are applied as follows: Bottom nodes of the lower loading clevis are fixed in all directions and those of the upper loading clevis are allowed to move along the machine loading axis, i.e., the vertical direction, only. The test load is applied on the upper loading clevis in the vertical direction. After performing the stress analysis of the whole assembly, displacements are taken from nodes of the contact surfaces of the specimen to follow a submodeling procedure. These displacements along with element and node lists of the specimen model and those of the 3-D crack front are used in FRAC3D solver to compute SIFs along the crack front. FRAC3D solver [41] is part of Fracture and Crack Propagation Analysis System (FCPAS) [42] as a standalone finite element program and employs enriched finite elements to compute the resulting SIFs. The enriched finite elements do not require special mesh near the crack front and the SIFs along the crack front are directly solved for at the same time as nodal displacements without any post-processing effort.

Crack growth model of Paris-Erdogan [43,44] law as shown in Eq. (1) is used for prediction of nodal crack growth increments,

$$\frac{da}{dN} = C(\Delta K_{eq})^n \tag{1}$$

where, a is the crack length, C and n are the crack growth material constants, N is the number of loading cycles and ΔK_{eq} is the equivalent SIF range under mixed mode fatigue loading. Material constants, which are obtained from multiple mode-I fatigue crack growth experiments according to ASTM E-647 [37] and representing the mean behavior of fatigue crack growth of the tested material under R = 0.1, are $1.46\text{x}10^{-6}$ for C and 2.44 for n (da/dN in mm/cycle and K in $\text{MPa}^*\text{m}^{1/2}$). The FCG simulation (Fig. 4) is performed by predicting the incrementally advancing 3-D crack front on a given state using numerical data in terms of mixed mode SIFs and local orientations for all nodes describing the crack front and material properties combined with growth criterion. This process is repeated until when the maximum allowed equivalent SIF value or the critical crack length is reached. Further theoretical details of the procedure is described in [42].

An improved empirical crack deflection angle equation (Eq. (2)) developed in a previous study by Demir et al. [36] is used for prediction of crack deflection angles on the crack front nodes.

$$\theta_0 = -\arccos\left(\frac{a\cdot K_{II}^2 + K_I\cdot\sqrt{K_I^2 + b\cdot K_{II}\cdot K_I} + c\cdot K_{II}\cdot K_I}{K_I^2 + d\cdot K_{II}^2}\right) \tag{2}$$

The coefficients of Eq. (2) are given in Table 1.

Recently developed 3-D equivalent SIF equations (Eqs. (3) and (4)) from a previous study by Demir et al. [18] are used to compute the alternating equivalent stress intensity factor under fatigue loading. The equations were developed using tens of data points from respective 3-D mixed mode fracture tests in terms of fracture loads and their corresponding SIFs representing the exact test conditions. In Eq. (3), first, using data from pure tearing experiments employing the compact tension tearing (CTT) specimen, a relationship is determined between the coupled mode-II and mode-III SIFs;

$$K_{eq(II-III)} = \sqrt{0.6890\cdot K_{II}^2 + 0.6796\cdot K_{III}^2} \tag{3}$$

Then, using data from fully 3-D mixed mode fracture tests in terms of fracture loads and their corresponding SIFs, in combination with Eq. (3), the following equation involving all modes of SIFs is defined to determine the equivalent SIF [18];

$$K_{eq} = \sqrt{a\cdot K_I^2 + b\cdot K_{eq(II-III)}^2 + c\cdot K_I K_{eq(II-III)}} + \left(d\cdot K_I^4 + e\cdot K_I K_{eq(II-III)}^3\right)^{0.25} \tag{4}$$

Table 1
Coefficients of crack deflection angle equation (Eq. (2)).

A	b	c	d
0.1723	5.1062	−2.7483	−1.1636

The coefficients of Eq. (4), which are obtained from nonlinear regression analyses of the mixed mode SIFs from all mixed mode fracture tests at the point of fracture, are given in Table 2 [18]. The developed criterion assumes that when the equivalent SIF (K_{eq}) given by Eq. (4) reaches mode-I fracture toughness (K_{Ic}) of the corresponding material, unstable crack growth and fracture occurs.

For comparison and to evaluate the accuracy of the developed criterion, crack propagation analyses are also performed by using the Maximum Tangential Stress (MTS) criterion proposed by Erdogan and Sih [45] and crack growth surfaces predicted using the developed and MTS criteria are compared with experimental results. Another commonly used measure for mixed mode facture problems is the Minimum Strain Energy Density (MSED) criterion [14]. Comparison with a reference using the MSED criterion is also presented in a validation problem involving 3-D mixed mode fatigue crack growth in a cylindrical specimen. According to the MTS criterion, crack extends from the crack tip radially in perpendicular direction to the maximum tangential stress. If this tangential stress exceeds a critical value or K_{eq} reaches the K_{Ic} value of the material considered, unstable fracture occurs.

Equivalent SIF (K_{eq}) and crack deflection angle (θ_0) for the MTS criterion are expressed by,

$$K_{eq} = \cos\frac{\theta_0}{2}\left[K_I \cos^2\frac{\theta_0}{2} - \frac{3}{2}K_{II}\sin\theta_0\right] \tag{5}$$

$$\theta_0 = -\arccos\left(\frac{3K_{II}^2 + K_I\sqrt{K_I^2 + 8K_{II}^2}}{K_I^2 + 9K_{II}^2}\right) \tag{6}$$

The following method is used to determine and quantify the difference between the crack growth surfaces obtained from experiments and numerical simulations. In Fig. 6, by aligning the pre-crack surfaces as the reference surfaces, the method for comparisons of experimental fatigue crack growth surfaces with those from numerical simulations combined with the developed and MTS criteria is presented for an arbitrary loading angle. Hundreds of line beams that are perpendicular to the pre-crack surfaces, i.e., parallel to the height of the specimen, are passed through the crack growth surfaces of the cracked part excluding sections in the close vicinity of free-surfaces. For each line beam, the intersection points with the experimental and numerically predicted surfaces and

Table 2
Coefficients of new developed equivalent SIF equation (4).

a	*b*	*c*	*d*	*e*
0.5263	0.3322	−0.1112	0.0257	−0.0004

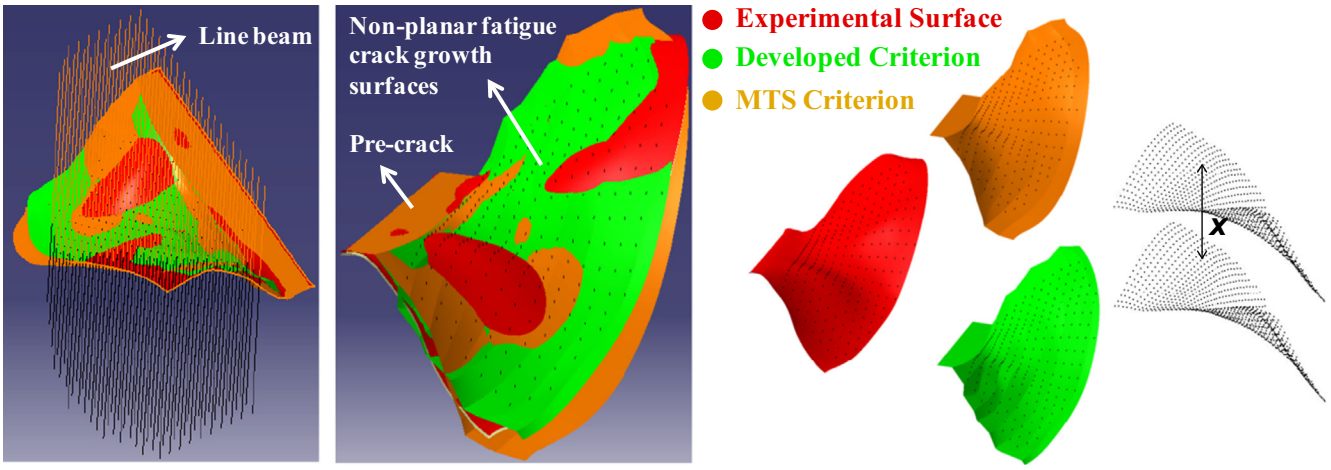

Fig. 6. Method for comparison of experimental and numerically predicted fatigue crack growth surfaces.

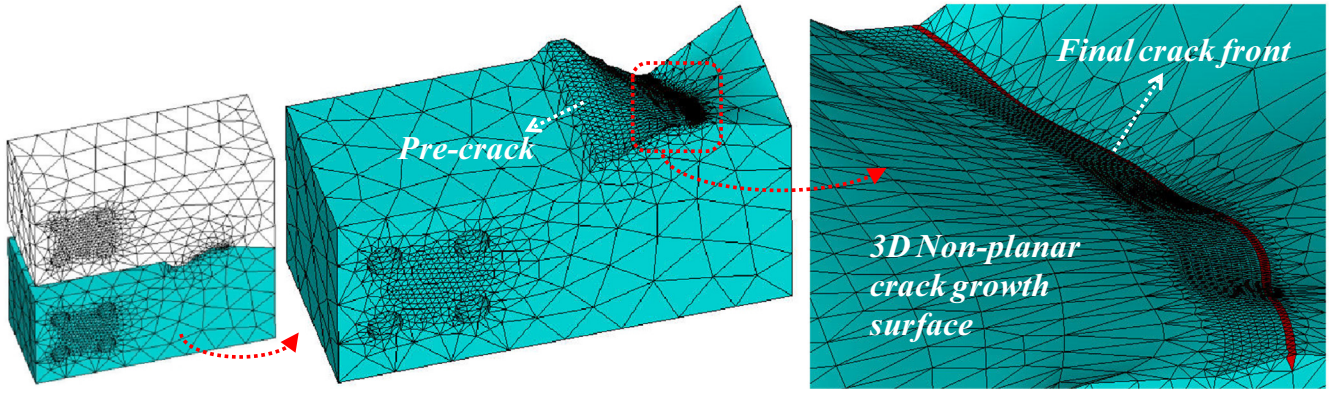

Fig. 7. Finite element mesh for model with predicted final crack front profile using the developed criteria, M−I/II = 45°, M−I/III = 45°, M−II/III = 45°.

their coordinates are determined. By calculating the vertical distances between the intersection points on the experimentally observed and numerically predicted surfaces for all line beams covering the crack growth surface, the root mean square (x_{rms}) value is defined using Eq. (7) given below.

$$x_{rms} = \sqrt{\frac{1}{n}\sum_{i=1}^{n} x_i^2} = \sqrt{\frac{x_1^2 + x_2^2 + \ldots + x_n^2}{n}} \tag{7}$$

Using the above equation, an average distance between the compared surfaces is calculated, which quantitatively allows assessing the deviations of the predicted crack surfaces from those obtained from the experiments. It is also noted that based on a previous sensitivity study [52] involving simulations of 3-D mode-I fatigue crack propagation problems, maximum incremental crack growth distances in the current simulations are taken as nearly one tenth of the total crack length.

3.2. Results of mixed mode-I/II/III fatigue crack growth analyses

Modeling and analyses of mixed mode-I/II/III crack growth experiments are performed for three different loadings. These are; M−I/II = 45°, M−I/III = 45°, M−II/III = 45°,which involves moderate level of mode mixity, M−I/II = 75°, M−I/III = 75°, M−II/III = 15° and M−I/II = 75°, M−I/III = 75°, M−II/III = 45°, which represent higher levels of mode mixity conditions. Fatigue crack growth analyses and experiments are performed at a stress ratio of R = 0.1 for all loading conditions.

Fatigue crack growth surface of the specimen tested under M−I/II = 45°, M−I/III = 45°, M−II/III = 45° loading is, first, scanned for modeling the actual pre-crack front and to determine the final crack front point at which unstable fracture occurs. The maximum applied fatigue load is F_{max} = 6.9 kN as in the experiment and the analyses are repeated until maximum computed equivalent SIF (K_{eq}) reaches the mode-I fracture toughness (K_{Ic}) of the material (29 MPa$\sqrt{m}$). Fig. 7 shows different views of the finite element model containing the final crack front profile predicted using the recently developed equivalent SIF and crack deflection angle criteria (Eqs. (2), 3 and 4). It is seen from the figure that fully tetrahedral mesh is used along the crack front and in the whole model. In Fig. 8, distributions of mixed mode three-dimensional SIFs along the crack fronts from back surface of the specimen towards the front surface for the initial and final stage of crack growth increments predicted by using, respectively, the MTS and the developed criteria are given. As expected, with the usage of both criteria K_{II} and K_{III} decrease with crack growth, while K_I increases. K_{II} SIF distribution along the crack front is nearly linear due to the counter rotations of the upper and lower crack faces in the out of plane direction of the specimen, which is activated by the remote mode-I/III component of the loading. It should also be noted, as seen from the SIF distributions, that the initially mixed mode fracture conditions for the planar pre-crack state is converged to that of a non-planar but merely a mode-I crack in the three-dimensional space, i.e., the growing crack surface evolved to a state nearly perpendicular to the loading axis. In Fig. 9, by aligning pre-crack surfaces as the reference surfaces, comparisons of predicted fatigue crack growth surfaces by the developed and the MTS criteria with the experimental crack growth surface are given from different views for the case of M−I/II = 45°, M−I/III = 45°, M−II/III = 45°. Surfaces predicted by using the developed and the MTS criteria are colored in green and orange, respectively, and the experimental surface is colored in red. Root mean square differences between the predicted crack propagation surfaces and the experimental fatigue crack growth surface for the described mixed mode loading conditions are presented in Table 3. It is seen from the table that the mean differences between the experimental surface and the surfaces predicted by the developed and the MTS criteria are, respectively, 1.02 mm and 1.48 mm for this loading angle. In other words, the developed criterion predicts the experimental surface better than the MTS criterion by reducing nearly one third of the latter's deviation from the actual experimental surface.

In Fig. 10, variations of mixed mode SIFs along the initial and final crack fronts obtained from crack growth predictions using the MTS and the developed criteria under M−I/II = 75°, M−I/III = 75°, M−II/III = 15° loading angles are given. For this case, fatigue crack growth analyses are performed under F_{max} = 12 kN fatigue load. Comparisons of fatigue crack growth surfaces obtained from the experiment with those from the numerical simulations by using the developed and the MTS criteria are shown in Fig. 11. The root mean square differences between the experimental surface and the surfaces predicted by the developed and the MTS criteria are, respectively, 0.46 mm and 0.50 mm (Table 3) for this loading condition. It is seen from Fig. 11 that the predicted and experimental crack growth surfaces are very close to each other for this loading case.

Finally, mixed mode-I/II/III fatigue crack growth experiments and numerical simulations are performed under F_{max} = 12 kN fatigue load for the case of M−I/II = 75°, M−I/III = 75°, M−II/III = 45°, which induces relatively higher mode-III condition along the crack front of the CTST specimen. Distributions of mixed mode SIFs along

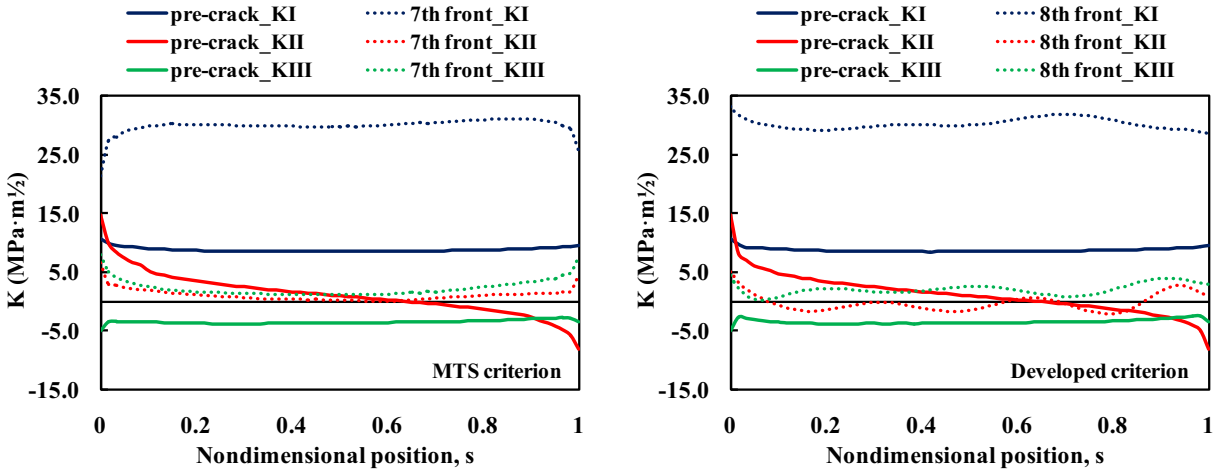

Fig. 8. Distributions of mixed mode SIFs along the crack fronts for initial and final crack fronts predicted by using the MTS and the developed criteria,M−I/II = 45°, M−I/III = 45°, M−II/III = 45°.

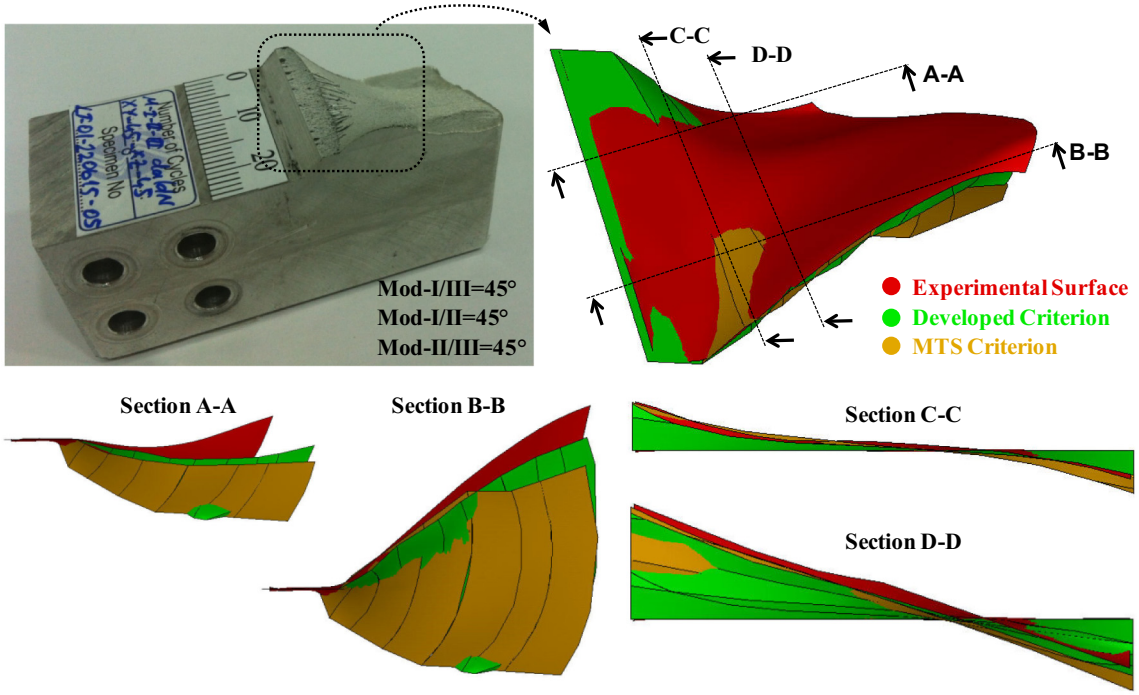

Fig. 9. Comparisons of fatigue crack growth surfaces from different views, M−I/II = 45°, M−I/III = 45°, M−II/III = 45°.

Table 3
Mean differences between predicted crack propagation surfaces and those from experimental measurements.

Loading Angles (°)			Mean Difference (from the experimental surface)		
M−I/II	M−I/III	M−II/III	MTS Criterion (mm)	Developed Criterion (mm)	Diff. %
45	45	45	1.48	1.02	45
75	75	15	0.50	0.46	9
75	75	45	1.42	0.76	87
0	45	0	0.49	0.39	26
0	60	0	0.49	0.55	−11
0	75	0	3.61	1.90	90

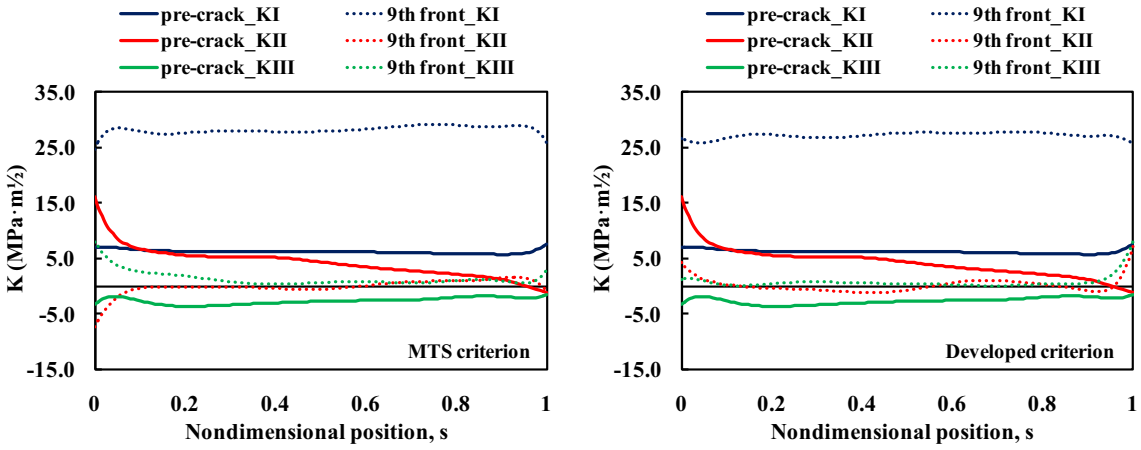

Fig. 10. Distributions of mixed mode SIFs along the crack fronts for initial and final crack fronts predicted by using the MTS and the developed criteria, M−I/II = 75°, M−I/III = 75°, M−II/III = 15°.

the initial and final crack fronts obtained from both crack growth simulations using the developed and the MTS criteria are given in Fig. 12. As seen from the SIF results for the pre-crack lengths, K_{II} and K_{III} are the initially dominant modes in this highly mixed mode loading condition compared to the two previous loading angles. In Fig. 13, comparisons of the fatigue crack growth surfaces are presented for different section views. It can be clearly seen from the figure that, the surface predicted by the simulation using the developed criterion is in very good agreement and, similar to the predicted surfaces from the previous loading conditions, shows

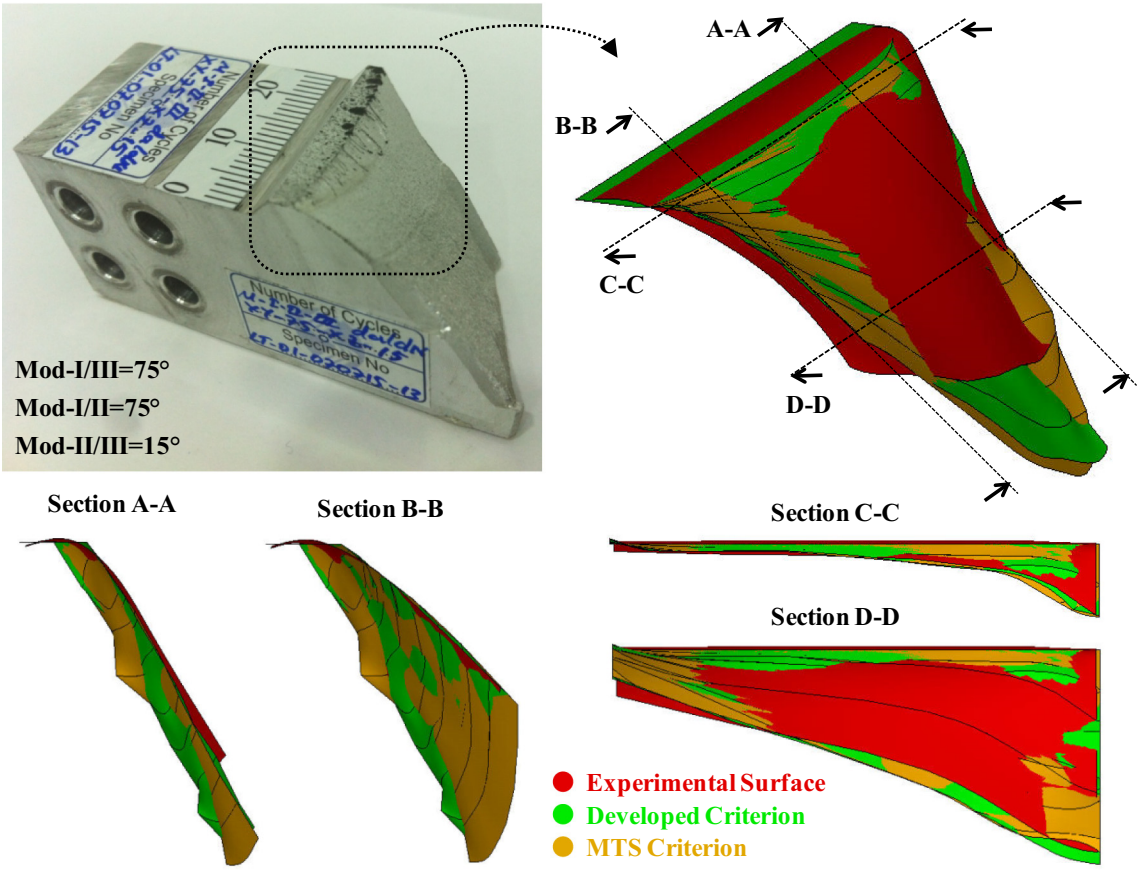

Fig. 11. Comparisons of fatigue crack growth surfaces from different views, M−I/II = 75°, M−I/III = 75°, M−II/III = 15°.

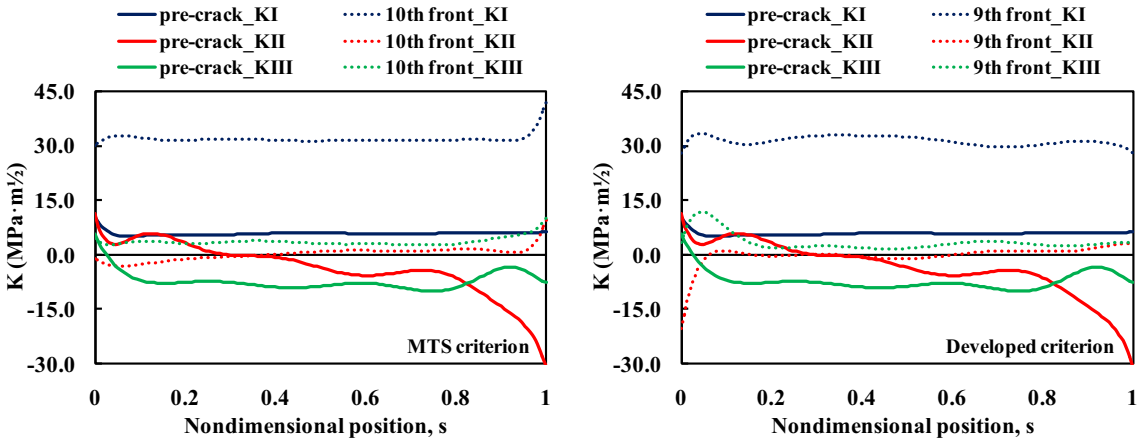

Fig. 12. Distributions of mixed mode SIFs along the crack fronts for initial and final crack fronts predicted by using the MTS and the developed criteria, M−I/II = 75°, M−I/III = 75°, M−II/III = 45°.

close tendency to the experimental surface. In this case, the developed criterion predicts the experimental surface better than the MTS criterion by reducing nearly half of the latter's deviation from the actual experimental surface (Table 3).

3.3. Application of the developed criterion to mixed mode-I/III fatigue crack growth experiments

In a previous study [46], numerical and experimental mixed mode-I/III fatigue crack growth analyses were performed using the same type of specimen made of the same material and crack growth surfaces predicted for mixed mode-I/III = 45°, 60° and 75° loading angles (Fig. 14) using the MTS criterion were compared with experimental measurements. In Fig. 14, the finite element model of mixed mode-I/III test assembly is given. The results showed that the predicted surface by MTS criterion starts to differ from the experimental surface for cases with loading angles equal to or greater than 75°, i.e., highly mode-III conditions. Much further details related to the mode-I/III crack growth modeling and experiments can be found in [46]. In this sub-section, to represent the applicability of the developed criterion, three-dimensional fatigue crack growth simulations are performed using both criteria for

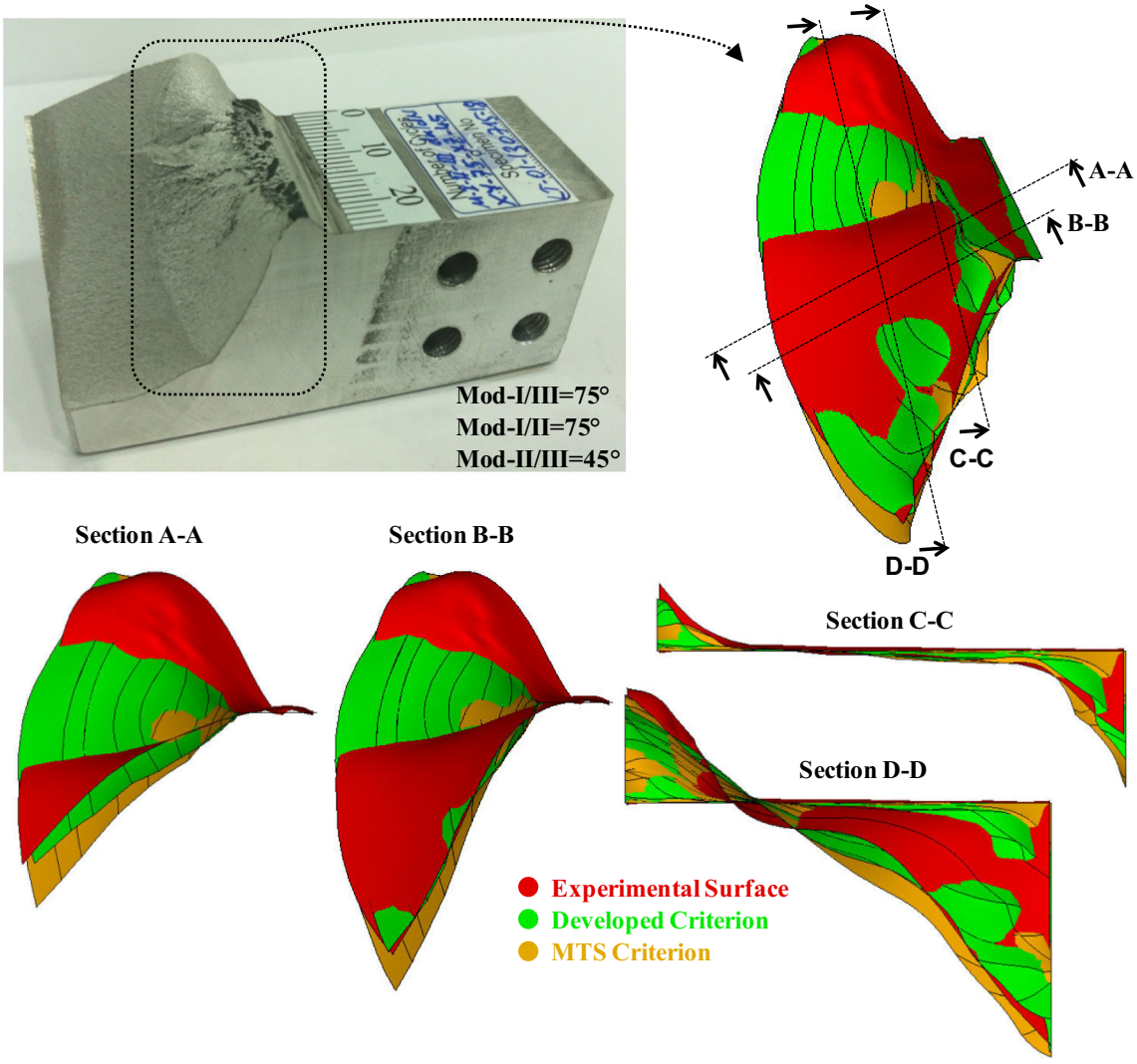

Fig. 13. Comparisons of fatigue crack growth surfaces from different views, M−I/II = 75°, M−I/III = 75°, M−II/III = 45°.

mixed mode-I/III loading angles equal to 45°, 60° and 75°. Crack growth surfaces predicted using the developed criterion are compared with the experimentally obtained surfaces and with the surfaces predicted by the MTS criterion, for which surface and life comparisons were presented in [46]. Fatigue crack growth analyses are performed at a stress ratio of R = 0.1 for all mixed mode-I/III loading conditions. First, crack propagation analyses are performed by applying F_{max} = 8 kN fatigue load as in the experiment under mixed mode-I/III loading angle of 45°. Distributions of mixed mode SIFs along the initial and final stage of crack fronts predicted by the developed and the MTS criteria are given in Fig. 15. It is seen that, K_{II} SIFs vary from negative to positive values anti-symmetrically with respect to the middle point of the crack front along the initial crack front due to the counter rotations of the crack faces in the out-of-plane direction of the specimen. By aligning pre-crack surfaces as the reference surfaces, comparisons of fatigue crack growth surfaces obtained from the experiment and the numerical analyses by using the developed and the MTS criteria are shown in Fig. 16. Good agreement between the predicted crack growth surfaces using both criteria and the experimental surface is evident for this loading condition. Root mean square differences between the experimental surface and the surfaces predicted by the developed criterion and the MTS criterion are 0.39 mm and 0.49 mm, respectively (Table 3).

The second comparison in this category of mixed mode loading type involves mixed mode-I/III loading angle of 60°. In the same manner as the previous test cases, crack propagation analyses are performed with a fatigue load of F_{max} = 10 kN. Distributions of SIFs along the initial and final predicted crack fronts and comparisons of the fatigue crack growth surfaces predicted by the MTS and the developed criteria with the experimentally measured surface are given in Figs. 17 and 18, respectively. It can be clearly seen from Fig. 18 that the predicted and experimental surfaces are very close to each other for this case, which involves relatively higher mode-III condition with respect to the previous case. Although they are considerably close to each other, the MTS criterion predicts the experimental surface slightly better than the developed criterion (Table 3).

Finally, mixed mode-I/III fatigue crack growth analyses are performed by using the developed criterion under F_{max} = 12 kN fatigue load to simulate the experiment with the loading angle of M−I/II I = 75°. Distributions of the SIFs along the initial and final crack fronts and comparisons of fatigue crack growth surfaces are given in Figs. 19 and 20, respectively. For this highly mixed mode-I/III situation, considerable differences are observed between the crack growth surface predicted by the simulation employing the MTS criterion and the experimental surface. Root square mean differences between the experimental surface and the surfaces predicted by

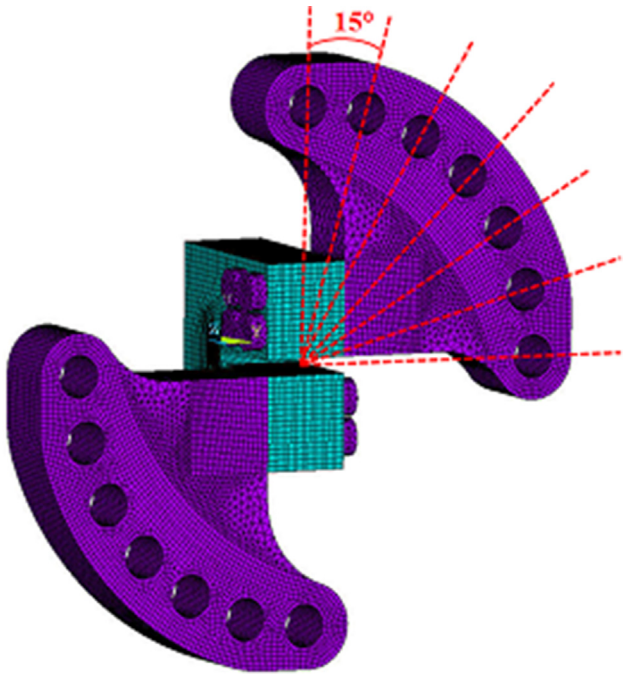

Fig. 14. Finite element model of mode-I/III fracture and FCG test assembly [46].

the developed criterion and the MTS criteria are 1.90 mm and 3.61 mm, respectively (Table 3). In this highly mixed mode case also, the developed criterion predicts the experimental surface better than the MTS criterion by reducing nearly half of the latter's deviation from the actual experimental surface.

4. Comparisons of mixed Mode-I/II/III fatigue lifes

One of the most important objectives of fatigue crack growth simulations is to be able to accurately predict the fatigue life of the component or the structure analyzed. In an effort to investigate the capability of the simulation process and the criterion presented in this study with respect to fatigue life prediction, crack growth lives are calculated for the problems presented so far, including comparisons with predicted lives from other fracture criteria in the literature. For the fatigue lives predicted by other 3-D mixed mode criteria in the literature, the mixed mode SIFs of the crack front mid-point obtained from the incremental crack propagation analyses by the developed criterion are used. Comparisons of the accumulated number of load cycles as a function of crack lengths using different criteria with experimental results are given in Fig. 21 for the case of M−I/II = 45°, M−I/III = 45°, M−II/III = 45°. Crack lengths on the predicted FCG lives represent the curve lengths of the mid-point of the crack front and are calculated by cumulatively adding up the distances between the mid-points of the simulated crack fronts in an incremental manner. Since crack length can not be measured for mid-thickness points during the experiments by using high-zoom cameras, to be compatible with the crack length definition on the predictions, the crack length data observed on the front and back surfaces of the specimen is scaled to represent the crack length in the mid-plane of the specimen by taking the corresponding mid-points on the pre-crack and the fast fracture crack front curves as the beginning and final crack lengths on the final broken surfaces. As seen from the figure, all criteria underestimate the experimental fatigue crack growth life, except the Kikuchi criterion, which has an error of approximately 10%. In Fig. 22, number of load cycles vs. crack lengths are shown for M−I/II = 75°, M−I/III = 75°, M−II/III = 15°. Again, all criteria underestimate the fatigue crack growth life with an error range of 25–50%. Finally, life comparisons are given (Fig. 23) for M−I/II = 75°, M−I/III = 75°, M−II/III = 45°, which is a highly mixed mode loading condition. It is clearly seen for this loading case that all of the criteria predict too short propagation lives compared to the experimental fatigue life, i.e., up to 6 times prediction errors exist. Although Kikuchi criterion shows relatively closer tendency to the experimental results during initial stages of the crack growth for the two previous loading cases, remarkable deviation exists from the experimental measurements, yielding up to 2 times prediction errors for this loading angle.

Similar results were also obtained [46] from the life comparisons for mixed mode-I/III loading conditions, which are not repeated here. In other words, all of the mixed mode criteria evaluated in the study predicted very short fatigue crack propagation lives under varying levels of out of plane mixed mode-I/III directions.

Many existing crack growth criteria assume that when the equivalent SIF (K_{eq}) reaches mode-I fracture toughness (K_{Ic}) value of the corresponding material, unstable fracture occurs. If one is to examine all K_{eq} levels in this study corresponding to final crack lengths for all mixed mode-I/II/III and mixed mode-I/III crack propagation analyses, as expected, equivalent SIFs are close to K_{Ic} of the material (29 MPa$\sqrt{m}$) corresponding to the L-T orientation. This states that the presented methodology can accurately predict the final unstable fracture point. However, it is highlighted that

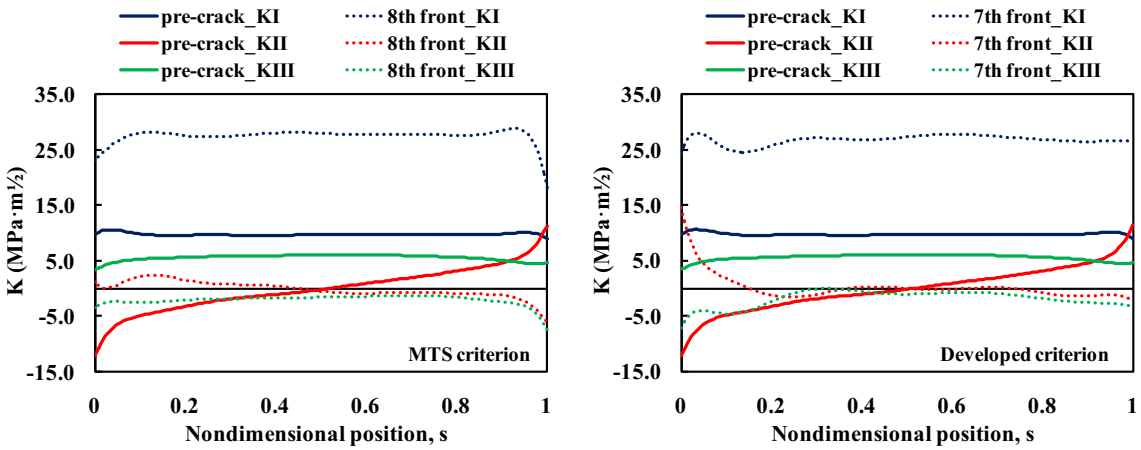

Fig. 15. Distributions of SIFs along the crack fronts for initial and final crack fronts predicted by using the MTS and the developed criteria, M−I/III = 45°.

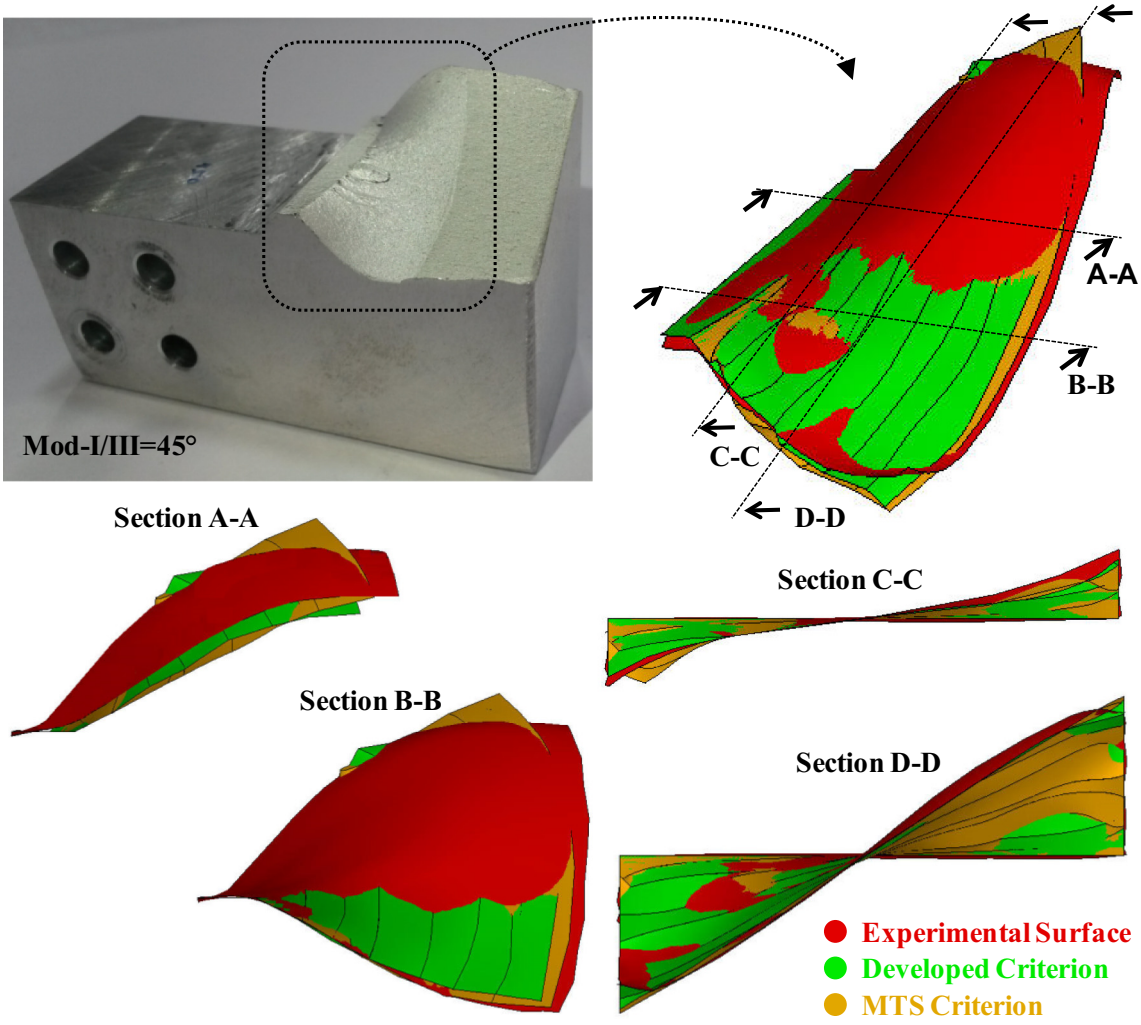

Fig. 16. Comparisons of fatigue crack growth surfaces from different views, M−I/III = 45°.

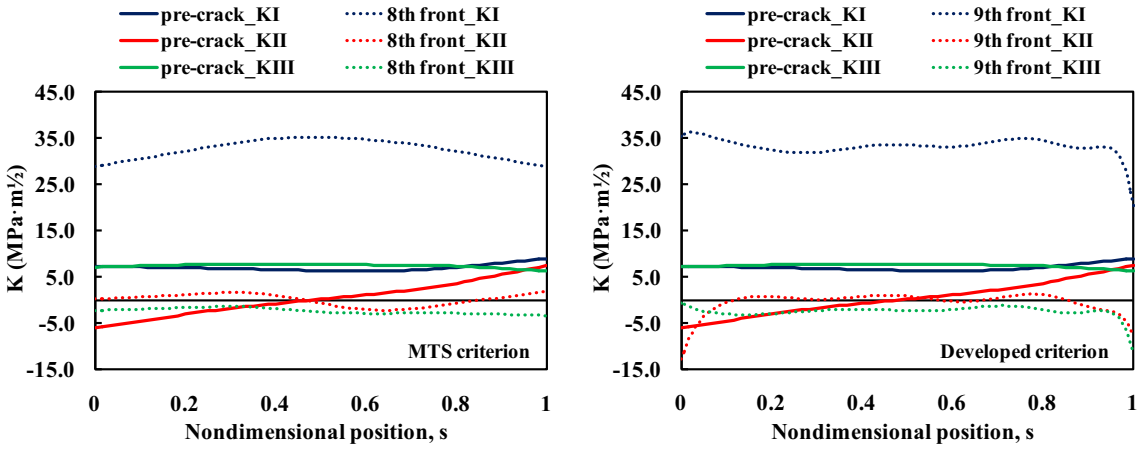

Fig. 17. Distributions of SIFs along the crack fronts for initial and final crack fronts predicted by using the MTS and the developed criteria, M−I/III = 60°.

although close predictions by the developed criterion are obtained for 3-D non-planarly evolving fatigue crack growth surfaces under all loading angles, predicted fatigue lives using the developed and different existing criteria are far away from the experimental data. In what follows, further explanation and reasoning for this situation are provided.

It is well-known that in rolled structures, materials exhibit different microstructural and mechanical properties in different directions due to elongations of grains in the rolling directions and re-positioning of their boundaries. Usually, FCG material constants, *C* and *n*, obtained from mode-I fatigue crack growth experiments are used for mixed mode FCG predictions [47–50], as is the

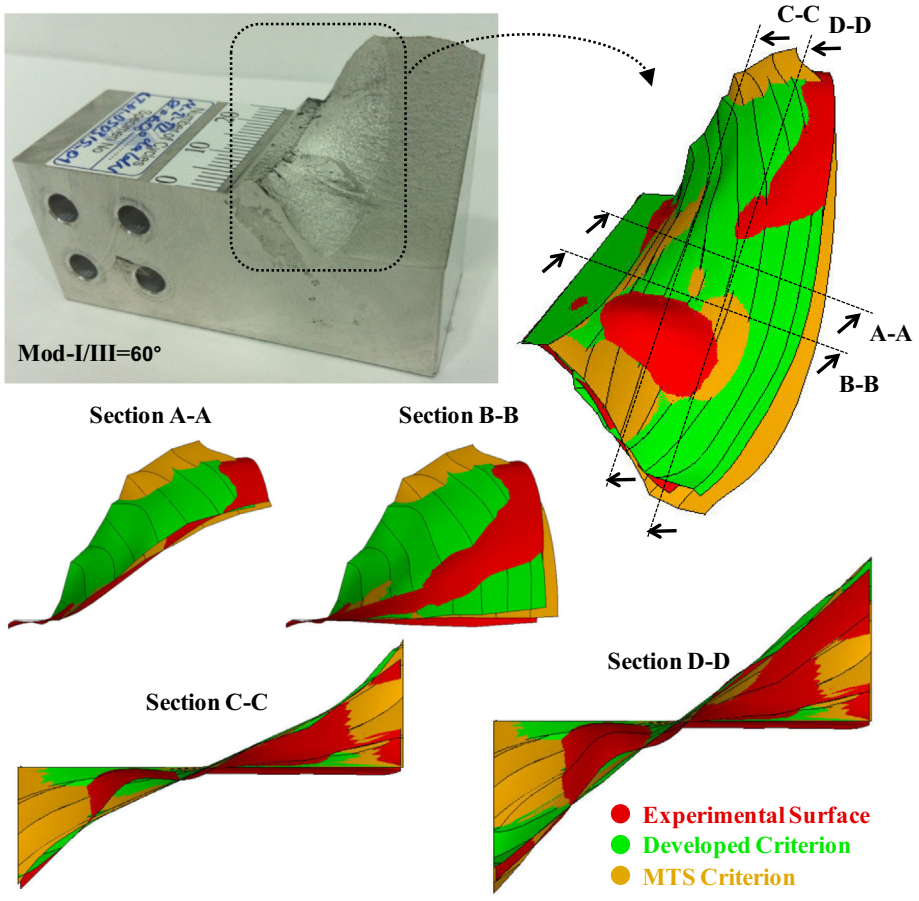

Fig. 18. Comparisons of fatigue crack growth surfaces from different views, M−I/III = 60°.

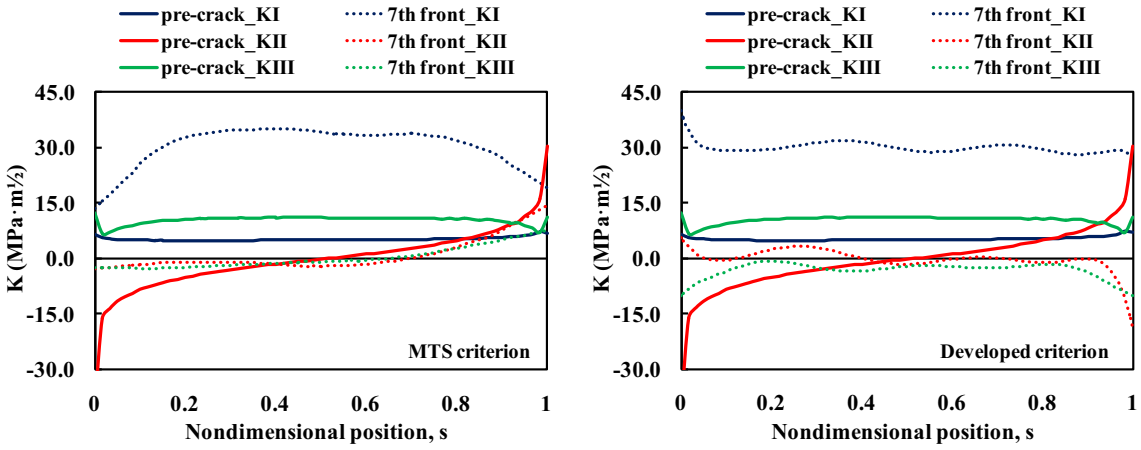

Fig. 19. Distributions of SIFs along the crack fronts for initial and final crack fronts predicted by using the MTS and the developed criteria, M−I/III = 75°.

case with this study. However, during 3-D mixed mode crack propagation, relative orientations of crack front points and those of local crack face surfaces along the crack front continuously change with respect to the rolling direction. Especially for highly mixed mode loading conditions, such as the loading cases analysed in this study, the orientations of crack front points and crack growth surfaces vary highly as clearly seen from all the predicted and experimentally obtained surface pictures. To illustrate, consider for example the case with M−I/II = 75°, M−I/III = 75°, M−II/III = 45° (Fig. 13), which exhibits a highly mixed mode-II/III loading condition on the specimen. It is seen from the figure that under this highly mixed mode loading situation, the crack tip deflects down with approximately 75° on the front surface of the specimen. Moreover, it is also observed that the FCG surface has an inclining slope in the out-of-plane direction towards the back of the specimen, resulting in truly 3-D non-planar evolved surface. Therefore, it can be conceived, by taking the crack direction notations in ASTM-E399 [30] as reference, that for the considered example

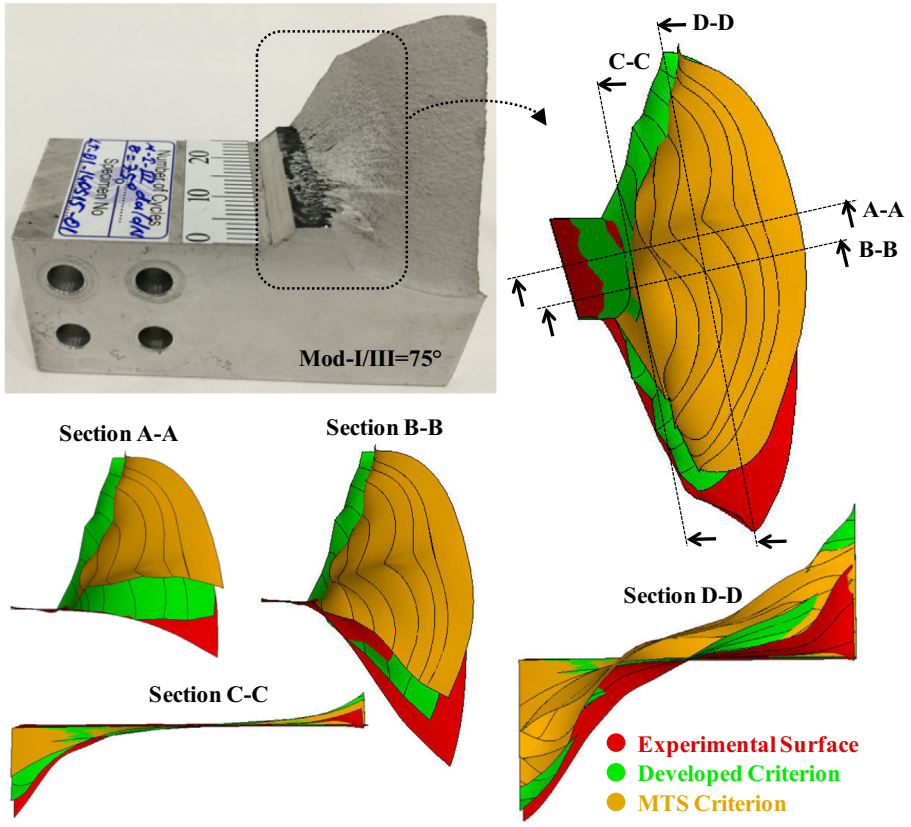

Fig. 20. Comparisons of fatigue crack growth surfaces from different views, M−I/III = 75°.

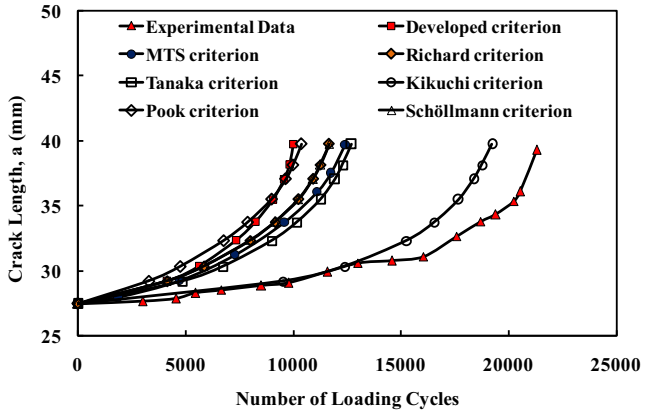

Fig. 21. Comparisons of fatigue crack growth lives, M−I/II = 45°, M−I/III = 45°, M−II/III = 45°.

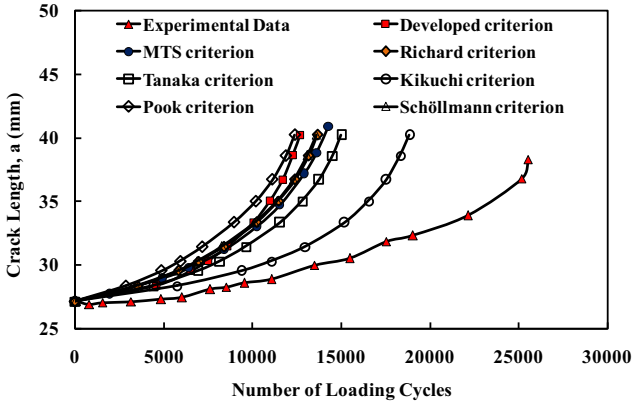

Fig. 22. Comparisons of fatigue crack growth lives,M−I/II = 75°, M−I/III = 75°, M−II/III = 15°.

and all others in this study, the evolving local crack surfaces along the crack front changes initially from L-T direction towards a mixed 3-D direction, simultaneously including T-L and S-T [30] orientations with varying levels along the crack front. Thus, as was indicated in [46], for accurate life prediction of mixed mode FCG problems, the crack growth material constants, *C* and *n*, corresponding to various 3-D directions of the non-planar crack surface profile along the crack front should be used for each crack propagation step. Needless to say that this involves multiple FCG tests at tens of different combinations of crack face rotations of the specimen with respect to the two independent rotation angles, i.e., from L-T towards T-L and S-T directions, including their combinations. This remains as a future study.

5. Validation of the developed criterion

Having presented the experimental and simulation results of 3-D mixed mode fatigue crack growth tests using the CTST specimen, in this section, the study performed by Citarella et al. [51] is considered as a test case for validation. Results from numerical analyses of three-dimensional fatigue crack propagation on a cylindrical steel bar with a straight-front edge notch under combined tension–torsion fatigue load is presented to demonstrate the application of the aforementioned analysis procedure and to validate the developed crack growth criterion. The initial crack dimensions given in Fig. 24 are L = 6.08 mm, h = 1.14 mm, a = 0.855 mm, b = 0.852 mm and c = 3.705 mm. The specimen material is carbon steel R2 M. For the combined tension–torsion fatigue crack growth

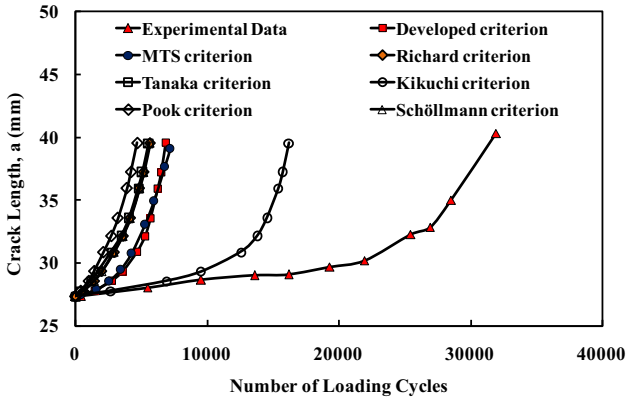

Fig. 23. Comparisons of fatigue crack growth lives,M−I/II = 75°, M−I/III = 75°, M−II/III = 45°.

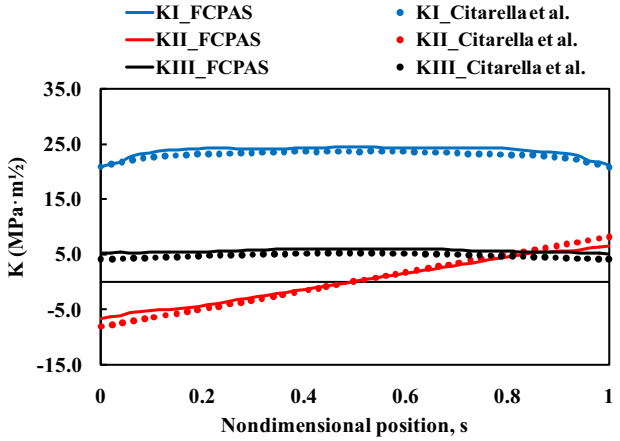

Fig. 25. Comparisons of SIFs obtained from FCPAS and from the study by [51] along the crack front for the initial crack front.

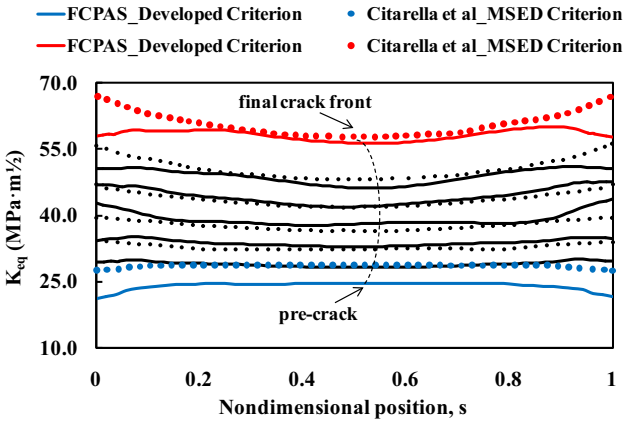

Fig. 26. Comparisons of equivalent SIFs along crack fronts predicted by using the developed criterion with Ref. [51].

analysis, loads are applied simultaneously such that in the no-notch and uncracked crossection, the maximum axial stress is 250 MPa and maximum shear stress is 100 MPa (R = 0.1). The fatigue crack growth-related material properties, C and n used in the analyses are $2.028 \cdot 10^{-9}$ (da/dN in mm/cycle and K in MPa$\sqrt{m}$) and 3.2046, respectively. Young's modulus and yield strength are E = 209 GPa and σ_y = 540.8 MPa [51]. As done for all the cases presented so far in this paper, fatigue crack growth analyses are performed using FCPAS. Comparisons of mixed mode three-dimensional SIFs along the crack front for the initial crack front obtained from FCPAS analysis and from the study by [51] are shown in Fig. 25. It can be clearly seen that distributions of SIFs are in close agreement with the reference data. Incremental crack growth analyses are terminated after 13 steps of crack propagation, whereas the number of propagation analysis steps is 10 in [51]. Comparisons of equivalent SIFs along the propagating crack fronts during FCG that are predicted using the developed criterion with the data of [51], which were predicted by minimum strain energy density (MSED) criterion [14], are given in Fig. 26. In the figure, the data from propagation steps 0, 2, 4, 6, 8 and 10 of the reference study [51] are plotted. Again, good agreement between the equivalent SIFs is achieved during crack propagation and at final crack front position.

Predicted fatigue crack propagation surface by FCPAS using the developed criterion is given in Fig. 27. As expected, an initially planar pre-crack surface becomes increasingly non-planar in the three-dimensional space, as the crack tip on one side deflects down and the other deflects up. Finally, comparison of fatigue crack growth lives predicted using the developed criterion with numerical and experimental data of Citarella et al. [51] is shown in Fig. 28. It is seen that crack growth life predicted by the developed criterion is in good agreement with the experimental data of [51].

6. Summary and conclusions

In this study, mixed mode-I/II/III fatigue crack growth experiments and corresponding numerical crack propagation simulations are carried out using the so-called Compact-Tension-Shearing-Tearing (CTST) specimen made of Al 7075-T651 aluminum alloy (L-T rolling direction) under different degrees of mixed mode loading conditions. The simulation analyses are performed using Fracture and Crack Propagation Analysis System (FCPAS), employing enriched crack tip elements to compute the 3-D SIFs. Applicability of a new 3-D fracture criterion developed in a previous study,

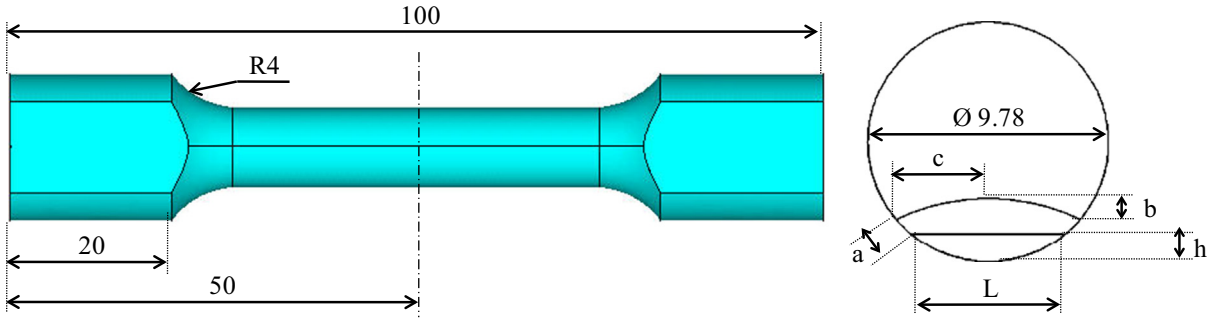

Fig. 24. Dimensions of cylindrical steel bar [51].

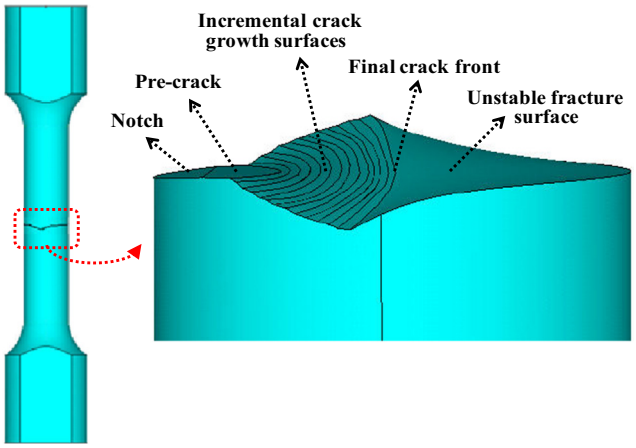

Fig. 27. Predicted fatigue crack propagation surface by FCPAS using the developed criterion.

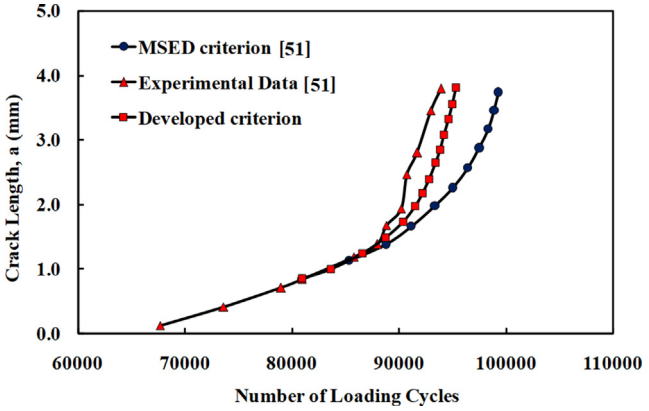

Fig. 28. Comparisons of predicted fatigue crack growth lives with the data of [51].

which proposed an equivalent SIF for unstable fracture, is also evaluated using the results of mixed mode-I/II/III experiments under fatigue loading. Moreover, the criterion is also applied to the previously performed mixed mode-I/III experiments. Predicted crack growth surfaces are compared with experimental measurements for different mode mixity ratios. Generally excellent agreement is observed between surfaces obtained from experiments and those predicted by the simulations using the developed criterion. It is seen from the results that, except one loading case (M−I/III = 60°), the developed criterion estimates the fatigue crack growth surface 9% to 90% better than the MTS criterion, when compared to the experimental data. Especially in such cases as high mode-mixity loading situations, the developed criterion predicts the experimental surface better than the MTS criterion by reducing nearly half of the latter's considerable deviation from the actual experimental surface. Comparisons of fatigue crack growth life predictions using existing and the developed criteria with experimental findings show that all of the mixed mode criteria evaluated predict very short lifetime for all mixed mode-I/II/III and I/III loading conditions. It is anticipated that this discrepancy between the predicted and experimental fatigue lives must be further looked into by using crack growth-related material constants, C and n, corresponding to the actual directions of three-dimensionally evolving crack front nodes on the non-planar crack profile during simulations. Finally, a validation example demonstrating the usage of the developed criterion is presented involving three-dimensional fatigue crack propagation on a cylindrical steel bar made of carbon steel and under combined tension–torsion fatigue load. The obtained results are compared to experimental crack growth data from the literature, which showed good agreement in terms of both evolving crack surface and fatigue crack growth life. Considering all of the above findings and comparative results, it is concluded that the presented methodology, employing three-dimensional enriched finite elements and the developed 3-D fracture criterion, is able to simulate three-dimensional mixed mode fatigue crack growth problems accurately and efficiently, especially in terms of evolving fatigue crack growth surfaces.

Declaration of Competing Interest

The authors declare that they have no known competing financial interests or personal relationships that could have appeared to influence the work reported in this paper.

Acknowledgement

The financial support by The Scientific and Technological Research Council of Turkey (TUBITAK) under Project Number: 113M407 and support by Dr. Sedat İriç during experiments are gratefully acknowledged.

References

[1] Nakamura T, Parks DM. Antisymmetrical 3-D stress field near the crack front of a thin elastic plate. Int J Solids and Struct 1989;25(12):1411–26.
[2] Richard HA, Kuna M. Theoretical and experimental study of superimposed fracutre modes I, II and III. Eng Fract Mech 1990;35:949–60.
[3] Pook LP. A note on corner point singularities. Int J Fract 1992;53(1):R3–8.
[4] Kotousov A. Fracture in plates of finite thickness. Int J Solids Struct 2007;44(25–26):8259–73.
[5] Kotousov A. Effect of plate thickness on stress state at sharp notches and the strength paradox of thick plates. Int J Solids Struct 2010;47(14–15):1916–23.
[6] Kotousov A, Berto F, Lazzarin P, Pegorin F. Three dimensional finite element mixed fracture mode under anti-plane loading of a crack. Theor Appl Fract Mech 2012;62:26–33.
[7] Kotousov A, Lazzarin P, Berto F, Pook LP. Three-dimensional stress states at crack tip induced by shear and anti-plane loading. Eng Fract Mech 2013;108:65–74.
[8] Berto F, Campagnolo A, Pook LP. Three-dimensional effects on cracked components under anti-plane loading. Frattura Integritá Strutturale 2015;33:17.
[9] Campagnolo A, Berto F, Pook LP. Three-dimensional effects on cracked discs and plates under nominal Mode III loading. Frattura Integritá Strutturale 2015:34..
[10] Pook LP. Comments and fatigue crack growth under mixed modes I and III and pure mode III loading. In: Miller KJ, Brown MW, editors. Multiaxial fatigue, ASTM STP853. Philadelphia: Amer. Soc. Test. Mat; 1985. p. 249–63.
[11] Richard HA, Schollmann M, Fulland M, Sander M. Experimental and numerical simulation of mixed mode crack growth. Proc. of 6th int. conf. of biaxial/multiaxial fatigue and fracture. 2001. p. 623–30.
[12] Schollmann M, Kullmer G, Fulland M, Richard HA. A new criterion for 3d crack growth under mixed mode (I+II+III) loading. Proc. of 6th int. conf. of biaxial/multiaxial fatigue and fracture. 2001. p. 589–96.
[13] Irwin GR. Analysis of stresses and strains near the end of a crack transversing a plate. J Appl Mech 1957;24:361–70.
[14] Sih GC. Strain-energy-density factor applied to mixed mode crack problems. Int J Fract Mech 1974;10:305–21. https://doi.org/10.1007/BF00035493.
[15] Tanaka K. Fatigue crack propagation from a crack inclined to the cyclic tensile axis. Eng Fract Mech 1974;6:493–507. https://doi.org/10.1016/0013-7944(74)90007-1.
[16] Kikuchi M, Wada Y, Ohdama C. Effect of KIII on fatigue crack growth behavior. J Eng Mat Tech 2012;134(4):041009. https://doi.org/10.1115/1.4006978.
[17] Ayhan AO, Demir O. A novel test system for mixed mode-I/II/III fracture tests–Part 1: Modeling and numerical analyses. Eng Fract Mech 2019;218:106597.
[18] Demir O, Ayhan AO, İriç S. A novel test system for mixed mode-I/II/III fracture tests–Part 2: Experiments and criterion development. Eng Fract Mech 2019;220:106671.
[19] Schirmeisen N-H, Richard HA. Weiterentwicklung der AFM-probe zur experimentellen analyse räumlicher mixed-mode-beanspruchung von Rissen. DVM-Bericht 241. Berlin: Deutscher Verband für Materialforschung und–prüfung e.V.; 2009. p. 211–20.
[20] Karpour A, Zarrabi K. Mixed-mode I/II/III fracture grip interface. Recent Pat Mech Eng 2010;3:131–9.

[21] Richard HA, Schramm B, Schirmeisen NH. Cracks on mixed mode loading theories, experiments, simulations. Int J Fat 2014;62:93–103.
[22] Zeinedini A. A novel fixture for mixed mode I/II/III fracture testing of brittle materials. Fatigue Fract Eng Mater Struct 2018:1–16.
[23] Razavi SMJ, Berto F. A new fixture for fracture tests under mixed mode I/II/III loading. Fatigue Fract Eng Mater Struct 2019:1–15.
[24] Benthem JP. State of stress at the vertex of a quarter-infinite crack in a half-space. Int J Solids and Struct 1977;13(5):479–92.
[25] Bažant ZP, Estenssoro LF. Surface singularity and crack propagation. Int J Solids and Struct 1979;15(5):405–26.
[26] Pook LP. On fatigue crack paths. Int J Fatigue 1995;17(1):5–13.
[27] Pook LP. Crack profiles and corner point singularities. Fatigue Fract Engng Mater Struct 2000;23:141–50.
[28] Pook LP. A 50-year retrospective review of three-dimensional effects at cracks and sharp notches. Fatigue Fract Engng Mater Struct 2013;36(8):699–723.
[29] Pook LP, Berto F, Campagnolo A. State of the art of corner point singularities under in-plane and out-of-plane loading. Engng Fract Mech 2017;174:2–9.
[30] ASTM. E399–17. Standard Test Method for Linear-Elastic Plane-Strain Fracture Toughness KIc of Metallic Materials. West Conshohocken, PA: ASTM International; 2018.
[31] She C, Guo W. The out-of-plane constraint of mixed-mode cracks in thin elastic plates. Int J Solds Struct 2007;44:3021–34.
[32] Hebel J, Hohe J, Friedmann V, Siegele D. Experimental and numerical analysis of in-plane and out-of-plane crack tip constraint characterization by secondary fracture parameters. Int J Fract 2007;146(173):188.
[33] Qian G, Gonzalez-Albuixech VF, Niffenegger M. In-plane and out-of-plane constraint effects under pressurized thermal shocks. Int J Solds Struct 2014;51:1311–21.
[34] Mu MY, Wang GZ, Tu ST, Xuan FZ. Three-dimensional analyses of in-plane and out-of-plane crack-tip constraint characterization for fracture specimens. Fat Fract Eng Mat Struct 2016;39:1461–76.
[35] Terfas OA, Kriama AM. Out-of-plane constraint based fracture toughness. Proceedings of the World Congress on Engineering, 2013; Vol III, WCE 2013, July 3 - 5, 2013, London, U.K.
[36] Demir O, Ayhan AO, İric S. A new specimen for mixed mode-I/II fracture tests: modeling, experiments and criteria development. Eng Fract Mech 2017;178:457–76. https://doi.org/10.1016/j.engfracmech.2017.02.019.
[37] ASTM E647-13a. Standard test method for measurement of fatigue crack growth rates. West Conshohocken, PA: ASTM International; 2015.
[38] Newman JC, Yamada Y. Compression precracking methods to generate near-threshold fatigue-crack-growth-rate data. Int J Fat 2010;32:879–85.
[39] James MA, Forth SC, Newman JA. Load History Effects Resulting from Compression Precracking. J ASTM Int 2005;2:JAI12025.
[40] ANSYS. Theory manual version 12.0. Canonsburg, PA, USA: Ansys Inc; 2009.
[41] Ayhan AO, Nied HF. Stress intensity factors for three-dimensional surface cracks using enriched elements. Int J Numer Method Eng 2002;54:899–921. https://doi. org/10.1002/nme.459.
[42] Ayhan AO. Simulation of three-dimensional fatigue crack propagation using enriched finite elements. Comput Struct 2011;89:801–12.
[43] Paris PC, Gomez MP, Anderson WE. A rational analytic theory of fatigue. The Trend Eng 1961;13:9–14.
[44] Paris PC, Erdogan F. A critical analysis of crack propagation laws. J Basic Eng-T ASME 1963:528–34.
[45] Erdogan F, Sih GC. On the crack extension of plates under plane loading and transverse shear. J Basic Eng 1963;85:519–27.
[46] Yaren MF, Demir O, Ayhan AO, İriç S. Three-dimensional mode-I/III fatigue crack propagation: computational modeling and experiments. Int J Fatigue 2019;121:124–34.
[47] Seo KJ, Choi BH, Lee JM, Shin SM. Investigation of the mixed-mode fatigue crack growth of a hot-rolled steel plate with a circular microdefect. Int J Fatigue 2010;32(7):1190–9.
[48] Boljanović S, Maksimović S. Mixed mode crack growth simulation with/without overloads. Int J Fatigue 2014;67:183–90.
[49] Sajith S, Shukla SS, Murthy KSRK, Robi PS. Mixed mode fatigue crack growth studies in AISI 316 stainless steel. Eur J Mech A-Solid 2019;103898.
[50] Sajith S, Murthy KSRK, Robi PS. Experimental and numerical investigation of mixed mode fatigue crack growth models in aluminum 6061–T6. Int J Fatigue 2020;130:105285.
[51] Citarella R, Lepore M, Shlyannikov V, Yarullin R. Fatigue surface crack growth in cylindrical specimen under combined loading. Eng Fract Mech 2014;131:439–53.
[52] Uslu M, Demir O, Ayhan AO. Surface cracks in finite thickness plates under thermal and displacement-controlled loads – Part 2: Crack propagation. Eng Fract Mech 2014;115:255–69.